Scilight

Photochemistry and Spectroscopy
https://www.sciltp.com/journals/ps

Article

Check for updates

Bridging Molecular and Periodic Models: A Theoretical Study of the Spectroscopic Properties of Polythiophene †

Carlo Saporiti [1], Matteo Tommasini [1], Daria Ruth Galimberti [2] and Chiara Castiglioni [1,*]

[1] Dipartimento di Chimica, Materiali e Ingegneria Chimica Giulio Natta, Politecnico di Milano, 32−20133 Milano, Italy
[2] Institute for Molecules and Materials, Faculty of Science, Radboud University Nijmegen, 6500 GL Nijmegen, The Netherlands
* Correspondence: chiara.castiglioni@polimi.it
† This article is dedicated to Prof. Giuseppe Zerbi in recognition of his outstanding scientific contributions to Spectroscopy.

How To Cite: Saporiti, C.; Tommasini, M.; Galimberti, D.R.; et al. Bridging Molecular and Periodic Models: A Theoretical Study of the Spectroscopic Properties of Polythiophene. *Photochemistry and Spectroscopy* **2026**, *2*(2), 1. https://doi.org/10.53941/ps.2026.100012

Received: 9 December 2025
Revised: 15 January 2026
Accepted: 21 January 2026
Published: 7 April 2026

Abstract: Polymeric organic semiconductors play a pivotal role in the development of new organic thermoelectric materials, sensing, and organic optoelectronics. Understanding the relation between their structure and properties is essential for designing the next generation of materials with improved features. Theoretical modelling based on first-principles calculations is a powerful aid for interpreting experimental structural and spectroscopic data of π-conjugated polymers, both in their pristine and doped states. Two approaches are currently available, i.e., oligomeric models and one-dimensional (1D) periodic crystal, each of one with its advantages and disadvantages. The combination of both allows to overcome the limitations of each. However, to do this, it is fundamental to systematically address the differences between these two approaches (molecular models vs. crystals). Here, we present a first systematic comparison between oligomeric and (1D) crystal models for describing the structural and spectroscopic properties of polyconjugated polymers. Using polythiophene (PT) and poly(3-hexylthiophene) (P3HT) as prototypical benchmark systems, we examine the relationship between finite-size oligomers and the corresponding infinite polymer treated as a one-dimensional (1D) crystal under periodic boundary conditions. Density functional theory (DFT) calculations are performed to examine the convergence of geometrical parameters and vibrational features (IR and Raman) as the oligomer length increases. The 1D crystal model is then evaluated as the limiting case of the oligomeric series. Its advantages in simplifying vibrational mode analysis are illustrated. This study establishes a methodological framework connecting molecular and periodic models, with direct relevance to the interpretation of experimental vibrational spectra of conducting polymers.

Keywords: polythiophene; poly(3-hexylthiophene), infrared and Raman spectroscopy; conducting polymers; DFT calculations; periodic boundary conditions

1. Introduction

Polymeric organic semiconductors, possessing an electronic structure with delocalized π-electrons along their backbone, can achieve high electrical conductivity through chemical doping processes [1–5]. Their major applications in the doped state include the development of organic thermoelectric materials, sensing, and organic optoelectronics [5–10]. The structure of conducting polymers typically consists of sequences of CC bonds in sp^2 or *sp* hybridization (as in polyacetylene or polyynes) or of aromatic and heteroaromatic rings (as in poly(p-phenylene), polythiophene, polypyrrole, etc.). The grafting of side chains—such as alkyl chains with tailored

length and structure—is a widely employed strategy to ensure good solubility and processability, as well as to promote the formation of supramolecular architectures in the solid state, favouring stability and efficient charge transport [11–18]. The engineering of polymer structures to achieve novel properties has relied on several additional strategies, including chemical substitution or the copolymerization of monomeric units with different electronic characteristics—for example, to obtain copolymers composed of alternating electron-donor and electron-acceptor monomers [19,20]. The introduction of polar bonds, for instance through fluorination, enables the formation of supramolecular structures characterized by strong electrostatic interchain interactions [21,22]. Conversely, the incorporation of bulky cyclic groups that wrap around the polymer backbone can isolate individual polymer chains, leading to a high anisotropy of transport properties along the chain axis [23,24]. Selective deuteration also modifies electron–phonon coupling and ultimately influences both the spectroscopic response and the electronic properties [25].

A key concept that has dramatically advanced the understanding of the physics and spectroscopic response of conducting polymers is the observation that molecules composed of finite sequences of identical chemical units (oligomers) progressively approach the properties of the ideally infinite polymer as their size increases [26–32]. This behaviour has been investigated through experiments on tailored molecules. The interpretation has been supported by finite-size molecular models, in which, however, the number and nature of units must be chosen to balance accuracy and computational cost [33–39]. An alternative approach models the macromolecular polymer as an ideal crystal, assuming conformational regularity and neglecting terminal effects, which, however, can be present in real polymers.

Poly(3-hexylthiophene) (P3HT) is one of the most widely studied and versatile conducting polymers, extensively employed in both its neutral and p-doped forms. Despite the vast literature on the structural, spectroscopic, and electronic properties of P3HT [11,12,40–51], theoretical models—often essential for interpreting experimental evidence—remain constrained by the need to simplify the systems under study, largely due to computational costs [33–39,43,44,52–54]. In the past, several authors have applied solid-state physics methods and formalisms to describe the characteristic spectroscopic features of conducting polymers and to establish relationships between charge-transport properties and material structure, with particular attention to the doped state and the peculiar physics of the charge carriers [55–59].

The characterization of P3HT, both in the pristine and p-doped states, largely relies on UV–Vis, Raman, and IR spectroscopies. Numerous works modelled its spectroscopic properties through density functional theory (DFT) calculations on oligomers of polythiophene (PT) and P3HT [36–39,43,44]. Simulations describing P3HT as an ideal crystal have also been reported and have revealed several crystalline phases of P3HT, in both neutral and doped states [60,61]. However, to the best of our knowledge, no studies have systematically addressed the limitations of these two approaches (molecular models vs. crystal) or evaluated the predictive capability of the crystal approach for the spectroscopic response. While oligomeric models are well understood and have successfully supported the interpretation of several experimental observations, the ideal crystal model—being a more realistic representation of the solid-state material, or at least of its crystalline phase—deserves further investigation.

In this work, we systematically compare the infinite model and a series of oligomers to provide a comprehensive characterization of the structural and spectroscopic behaviour of P3HT, as prototypical benchmark system. The polymer will be treated as a one-dimensional (1D) crystal, representing the infinite-length limit of isolated molecules of increasing size. This investigation lays the groundwork for developing a more realistic three-dimensional (3D) crystal model, with the ultimate goal of using periodic boundary condition (PBC) calculations to simulate the spectroscopic features of doped P3HT in synergy with molecular models. This combined approach will enable a rational interpretation of experimental evidence that cannot be captured by molecular methods alone—for example, solid-state effects arising from polymer-chain packing or the electron polarizability in an ideally infinite structure compared with confinement of π electrons in a finite-size molecule.

This paper has a methodological focus and begins by analysing the 1D crystal model in the simplest case of polythiophene (PT)—the parent polymer of P3HT, composed of an unfunctionalized chain of thiophene rings (side group R = H). Since it is known that in conjugated systems the onset of long-range interactions may require a unit cell larger than the minimal translational unit, we first examine the stability of the calculated results with respect to cell size. We then present a comparative discussion of the results obtained, at the same theoretical level, for PT oligomers of increasing length (from T4 to T45) and the infinite polymer. The discussion aims to address the following questions:

- Do the structural and spectroscopic properties of the oligomers converge as the monomer sequence length increases? Based on this, what is the threshold length (N) for a TN oligomer that can be considered a good model of PT? Since our focus is on vibrational spectra, the analysed parameters include geometry, IR, and Raman spectra (vibrational frequencies and intensities).

- Does the ideally infinite 1D crystal represent a good model for the study of the spectroscopic response of the real polymer in the solid state?

Being able to use the 1D crystal model confidently offers significant advantages—not least the drastic simplification of spectral analysis, due to the reduction of degrees of freedom to those of the elementary cell (for instance, the analysis of vibrational eigenvectors becomes both simpler and more robust). Moreover, it enables the investigation of the effects of introducing side-chains at a lower computational cost than that required for treating large molecular models.

Besides, a well-founded and carefully considered selection of molecular models will allow us to explore the effects of conformational changes (e.g., deviations from planarity) and the presence of defects, which cannot be captured in periodic structures but are nevertheless relevant in polymer solutions or amorphous phases.

In this work, we focus exclusively on the pristine (undoped) polymer. Following the systematic comparison between PT and its oligomers (TN), we extend the analysis to the comparison between the 1D crystal model of P3HT and its 3HT8 oligomer—a 3-hexylthiophene octamer used as a reference model in other studies [36].

2. Methods

All the DFT calculations discussed in this work have been performed using the B3LYP functional and are based on structural models mimicking the crystalline phase of P3HT in the solid state, where the thiophene backbone is reported to be fully planar [11–15,61]. For this reason, the geometry optimization is performed on planar structures. We consider the following structural models:

(1) Unsubstituted one-dimensional (1D) infinite crystal, indicated as PTn, with n number of thiophene rings—all in trans conformation—in the repeating unit cell (n = 2, 4, 6, 8). The calculations are carried out with periodic boundary conditions (PBC) and the cases n = 4, 6, 8 are supercells of the minimal translational unit (n = 2). The n thiophene rings in the guess geometry are taken from the corresponding n central units of a 12-rings oligothiophene, previously optimized with C_{2h} symmetry constraint in the absence of PBC. The calculation for that oligomer was performed by imposing co-planarity of the thiophene rings (i.e., all inter-ring C–C torsional angles fixed at $\theta = 180°$).

(2) Unsubstituted finite thiophene oligomers, indicated as TN, with N being the number of thiophene rings—all in trans conformation—constituting the molecular backbone (N = 4, 6, 8, 12, 14, 18, 22, 45). The guess geometry for the optimization procedure of the oligomers was derived from previously DFT optimized planar oligothiophenes [36] with the same number of thiophene rings.

(3) Alkyl-substituted models with a substitution pattern (position 3) matching a regioregular P3HT chain. The 1D crystal model of P3HT contains two alkylated thiophene rings in the unit cell, and its guess geometry is obtained from the previously optimized structure of the central unit of an octameric molecular model (3HT8).

All calculations reported in this work have been performed using the POB triple-zeta valence + polarization basis set for solid state systems, namely the POB-TZVP-rev2 basis set [62].

All the calculations regarding the 1D infinite crystal models have been performed with the CRYSTAL17 package [63–65], either imposing or neglecting the symmetry. The unsubstituted models belong either to the C_{2h}^1 or $P2/m11$ group, whereas the alkyl-substituted models belong either to the C_2^2 or $P112_1$ group, according to the Schoenflies or the Hermann-Mauguin notation, respectively. In addition, for the PT2 model, we evaluate the effects of the TOLINTEG and SHRINK parameters by comparing results obtained with the settings TOLINTEG (9 9 9 18) and SHRINK (8 8), with (12 12 12 24) and (16 16), respectively.

To assess convergence toward the properties of the 1D polymer, the CRYSTAL17 code has also been used to perform calculations on the oligothiophene molecular models (except for the T45 model). In this case, symmetry is exploited by imposing the C_{2h} (z) (Schoenflies) or $2/m$ (z) (Hermann-Mauguin) point group.

To perform the calculations in the absence of PBC, we have used the Gaussian09 package [66] on thiophene oligomers 3HT8 and TN (including the T45 model). It is important to notice that the implementation of B3LYP in CRYSTAL17 and Gaussian09 differs slightly. Notably, the Vosko-Wilk-Nusair correlation potential [67] included in the B3LYP definition [68,69] exists in different formulations: Gaussian09 adopts functional form III [66], whereas CRYSTAL17 adopts functional form V [65]. As illustrated below, this slight difference in the correlation potential causes minimal systematic differences in the vibrational properties of the models investigated in this work. Where necessary, to clarify this minor difference in the computational setup, we indicate the DFT functional as B3LYP-III or B3LYP-V.

Molecular structures for each model were fully optimized, and the final equilibrium structures used for the vibrational frequency calculations. IR and Raman spectra were computed in double harmonic approximation at

the same level of theory used for the geometry optimization. The vibrational analysis was carried out by means of a post-processing procedure using the Gaussian and CRYSTAL output files, following the method illustrated in [36].

3. Modelling Unsubstituted Polythiophene (PT) and Its Oligomers

3.1. PT as a One-Dimensional (1D) Crystal

We model the polymer chain as a one-dimensional crystal consisting of a periodic repetition along the chain axis $\boldsymbol{c}$ of a base unit composed of two co-planar thiophene rings (T2). Since this study aims to assess the convergence of characteristic parameters (equilibrium geometry, vibrational frequencies, and intensities) of oligomers of increasing length toward those obtained for the 1D crystal, it is first necessary to evaluate the extent to which the numerical values of the crystal parameters vary upon modifying the computational setup, once the functional and basis set have been selected. In systems with delocalized electrons—where long-range interactions are significant—the following aspects may affect the results:

i. Effect of the unit cell size: It is well known that the use of a supercell, i.e., a cell that is a multiple of the minimal translational unit, may influence the accuracy of periodic calculations since it affects the way long-range interactions are evaluated. To assess this effect, we tested the stability of our results by comparing supercells of double (PT4), triple (PT6), and quadruple (PT8) size with respect to the conventional cell containing a single T2 unit.
ii. Effect of symmetry: by enforcing the correct chain symmetry (C_{2h}), the *CRYSTAL* code allows describing the crystal structure based on a single asymmetric unit (i.e., one thiophene ring for the PT2 model). This choice helps to reduce numerical noise arising from minor differences in the description of the two rings forming the translational unit and it may have non-negligible effects on both the optimized crystal geometry and the computed vibrational spectra. Moreover, the use of symmetry constraints drastically reduces the computational costs.
iii. Effect of the numerical accuracy in the evaluation of the Coulomb and exchange integrals: the accuracy in CRYSTAL can be systematically improved by tightening the truncation criteria through the TOLINTEG parameter set. The thresholds (9 9 9 18) are typically chosen as a compromise between precision and computational cost; however, in systems involving extended π-electron conjugation, such as polythiophene, the accurate treatment of long-range electrostatic and exchange interactions may require stricter settings. Therefore, we investigated to what extent tightening the integral tolerances (thresholds set to 12 12 12 24) affects the convergence of structural parameters, total energy, phonon frequencies, and IR/Raman intensities. This assessment is essential to ensure that the observed differences between finite oligomers and the 1D periodic crystal are not artifacts caused by insufficient integral accuracy. We also investigated the effect of modifying the SHRINK parameter in CRYSTAL, which defines the density of the reciprocal-space sampling grid. In particular, we increased its values from (8 8) to (16 16).

Table 1 summarizes the results obtained from the different tests exploring the possible effects of the computational setup, as discussed in points (i)–(iii). The selected parameters are those that will later be used in our analysis of the molecular models and in their comparison with the one-dimensional (1D) crystal model: bond lengths (R), cell parameter (c), wavenumbers (ν), and intensities (I) of the most intense CC stretching modes in the IR spectrum (antisymmetric C=C stretching, *R*–) and in the Raman spectrum (collective CC stretching, assigned to the Effective Conjugation Coordinate mode—see below and [36,70–75]). For calculations performed using supercells, IR and Raman intensities are normalized to the smallest translational unit (T2). Figure 1 shows the IR and Raman spectra calculated using different computational setups, highlighting the effects of the symmetry constraint and the supercell approach. All spectral features are described consistently across all tests. From the data reported in Table 1, it can be verified that variations in CC bond lengths across the different calculations occur only at the fourth decimal place. We observe maximum deviations of 5% in the computed IR and Raman intensities and of 0.8 cm^{-1} in the vibrational frequencies. The symmetry constraint does not affect the numerical results, confirming that, when possible, it should be introduced in calculations to reduce the computational effort.

Since these variations are extremely small, definitely much smaller than the experimental uncertainty in the determination of the parameters of interest, we conclude that the (TOLINTEG (9 9 9 18), SHRINK (8 8)) computational setup with the minimal translational unit (PT2) can be confidently adopted to investigate the structural and spectroscopic features of PT properly. From this point onward, all analyses and comparisons will be carried out using this computational setup for the 1D crystal model. The above analysis is also essential in view of future extensions of the present modelling approach to systems characterized by larger translational units—such as polythiophenes with alkyl side chains, three-dimensional crystals comprising multiple polymer chains per unit

cell, doped polythiophene systems, or other conducting polymers with a larger and more complex monomeric unit—which would substantially increase the computational demand.

Table 1. Geometric and spectroscopic parameters of polythiophene computed at DFT (B3LYP-V/POB-TZVP) level for the one-dimensional (1D) crystal model, employing different computational setups (see text for details).

Computational Setup		R_{CC} (ring) Å	$R_{C=C}$ Å	R_{CC} (Inter-Ring) Å	R_{CS} Å	c Å	ν_{IR} (*R*–) cm^{-1}	I_{IR} (*R*–) km mol^{-1}	ν_{Raman} (ECC) cm^{-1}	I_{Raman} (ECC) $Å^4$ amu^{-1}
cell size	PT2(nosym)	1.408	1.374	1.434	1.775	7.851	1537.2	445.1	1477.5	22.8
	PT4	1.408	1.374	1.434	1.775	7.851	1537.1	441.2	1477.3	23.6
	PT6	1.408	1.374	1.434	1.776	7.851	1537.2	444.6	1477.3	23.9
	PT8	1.408	1.374	1.434	1.775	7.851	1537.2	444.2	1477.4	23.8
	PT2 (sym)	1.408	1.374	1.434	1.775	7.850	1537.3	445.0	1477.6	22.8
	TOLINTEG = 12	1.408	1.374	1.434	1.776	7.851	1537.0	463.4	1477.8	24.0
	SHRINK = 16	1.408	1.374	1.434	1.775	7.851	1537.2	443.2	1477.0	23.8

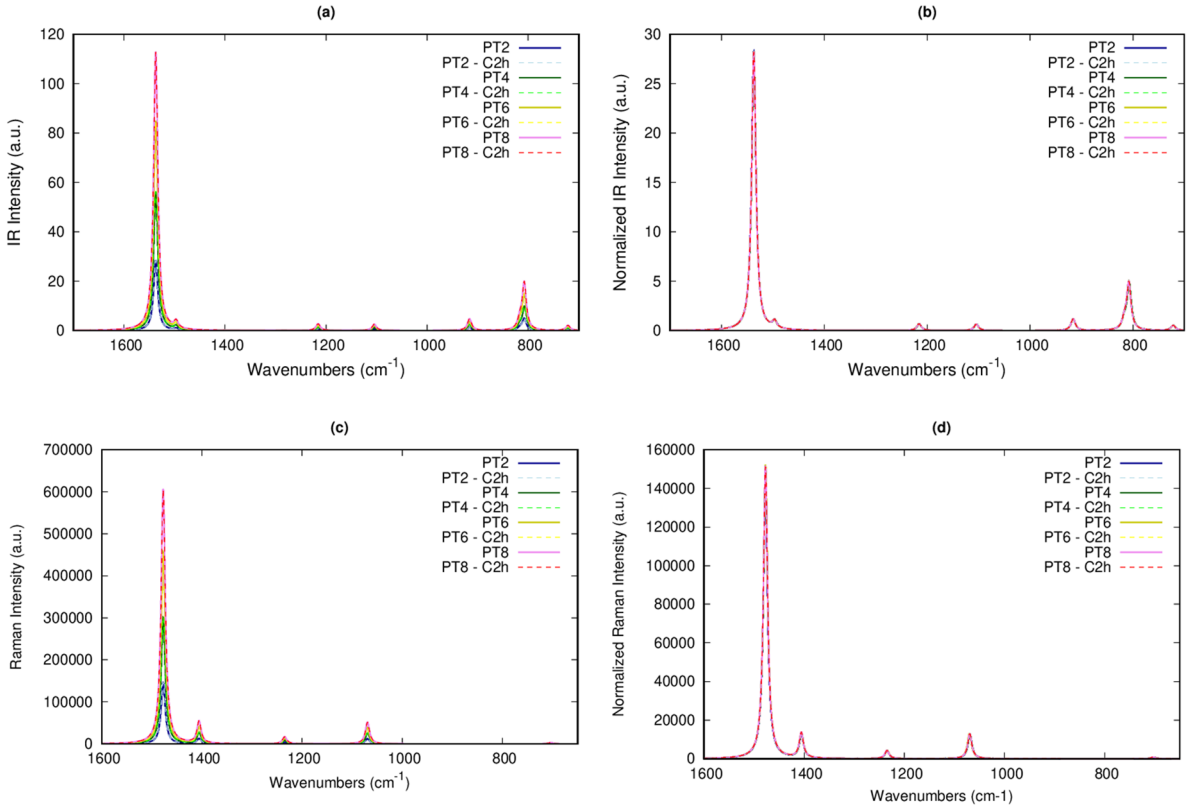

Figure 1. IR spectra (panel (**a**)) and Raman spectra (panel (**c**)) of polythiophene (1D crystal), calculated at DFT (B3LYP-V/POB-TZVP) level, using different DFT input setups with periodic boundary conditions (PBC) (see text). Panels (**b**,**d**) display the IR and Raman spectra, respectively, normalized to the number of T2 units within the translational cell adopted for each calculation. Spectra obtained by calculations with and without symmetry constraints, represented by solid and dashed lines respectively, are reported.

The optimized PT structure shows that the sequence of CC bonds forming the polymer backbone alternates between quasi-single and quasi-double bonds. However, the significant aromatic character of the thiophene ring leads to a marked shortening of the intra-ring CC single bond compared with the inter-ring CC single bond, with a bond difference of 0.026 Å. This structure is usually described as aromatic, in contrast to the hypothetical quinoid limiting form, in which the inter-ring bonds are double, and the single/double character of the CC bonds within the thiophene ring is reversed. To complete the geometrical analysis, we observe that the CS bond length is very stable across all the computational setups.

The theoretical prediction of the spectrum for the 1D crystal enables an accurate assignment of vibrational normal modes by analysing the associated eigenvectors. This step is also essential for the subsequent comparison with the spectra of the oligomeric models. Table 2 reports the eigenvectors corresponding to the most intense IR and Raman-active modes, which correspond to phonons with wavevector $\boldsymbol{q} = \mathbf{0}$ belonging to the irreducible representations of species A_u and B_u (IR-active phonons) and A_g (Raman-active phonons). The selection of the

modes presented here, based on their intensities, does not include any modes of B_g symmetry, as these transitions are very weak in PT.

As evident from the data in Table 2, the IR spectrum is dominated by the antisymmetric stretching mode of the C=C quasi-double bonds of the thiophene rings, *R*– at 1537 cm^{-1}. On the other hand, the Raman spectrum is primarily dominated by the band at 1477 cm^{-1}, associated with the collective stretching of all the CC bonds along the polymer backbone, commonly referred to as the Effective Conjugation Coordinate (ECC) mode. Vibrations along the ECC coordinate modulate the degree of CC bond-length alternation, since it corresponds to an out-of-phase oscillation of the C=C and C–C bonds; it can thus be described as an oscillation between a more aromatic and a more quinoid molecular structure.

A large body of literature [70–75] discusses the definition of the ECC coordinate for various conducting polymers, where the presence of strong electron–phonon coupling for vibrational modes with high ECC character causes a pronounced sensitivity of the frequencies of ECC modes to the degree of π-electron conjugation along the polymer backbone. Moreover, the strong electron–phonon coupling accounts for the exceptionally high Raman intensity of the ECC modes, which is typically so large that other (non-ECC) transitions appear comparatively negligible. From the perspective of the spectroscopic response, the peculiar features of the ECC modes are precisely what make delicate the modelling of the polymer via finite-size molecular models. It is well known that π-electron conjugation is affected by confinement effects in finite systems. In this context, an important question naturally arises: what is the appropriate molecular model size required to accurately describe the characteristic spectroscopic features of the polymer? The following analysis will address this issue.

Table 2. Sketches of the vibrational eigenvectors corresponding to the normal modes of PT and P3HT described as 1D crystals. The modes exhibiting the largest IR or Raman intensities have been selected. Blue and green segments indicate bond stretching and contraction, respectively; the segment thickness is proportional to the contribution of each bond deformation to the vibrational eigenvector. Red arrows represent the direction of atomic displacements within the normal mode. Out-of-plane atomic displacements are illustrated by red and blue circles, whose radii are proportional to the magnitude of the displacement. For each selected mode, the calculated wavenumber, IR or Raman intensity, vibrational assignment, and symmetry species are reported.

	PT – 1D crystal	**P3HT – 1D crystal**
	IR modes	**IR modes**
	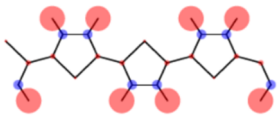	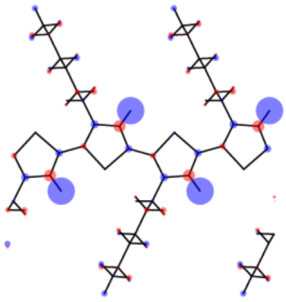
ν (cm^{-1})	808	855
I_{IR} (km mol^{-1})	75	21
Irrep – mode	A_u – CH out-of-plane bend	A – CH (ring) out-of-plane bend
	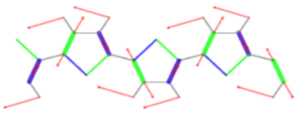	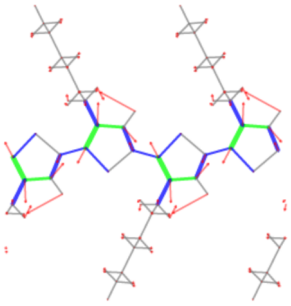
ν (cm^{-1})	1537	1550
I_{IR} (km mol^{-1})	445	247
Irrep – mode	B_u – antisymm C=C stretch, *R*–; CH wag	A – antisymm C=C stretch; CH wag

Table 2. *Cont.*

	PT – 1D crystal	P3HT – 1D crystal
	IR modes	**IR modes**
	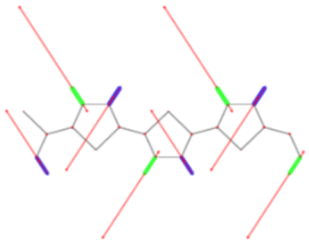	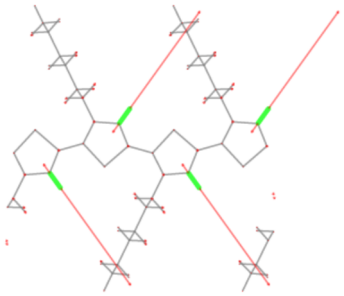
ν (cm^{-1})	3192	3186
I_{IR} (km mol^{-1})	63	107
Irrep – mode	B_u – antisymm CH stretch	A – CH (ring) stretching
	Raman modes	**Raman modes**
	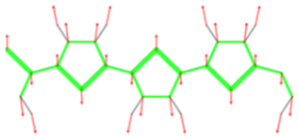	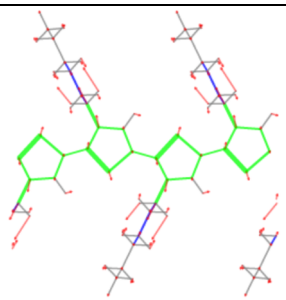
ν (cm^{-1})	703	609
I_{Raman} (10^3 Å^4 amu^{-1})	13	4
Irrep – mode	A_g – symm CS stretch	A – CS stretch
	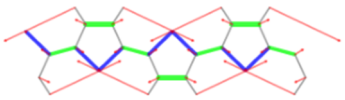	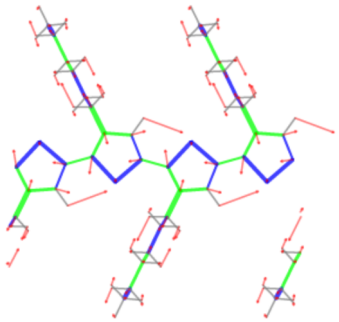
ν (cm^{-1})	1070	1043
I_{Raman} (10^3 Å^4 amu^{-1})	192	30
Irrep – mode	A_g – collective symm C–C stretch; CS symm stretch, CH wag	A: ring CC stretch + CC hexyl; CS stretch, CH wag
	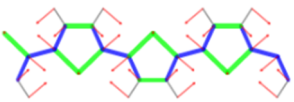	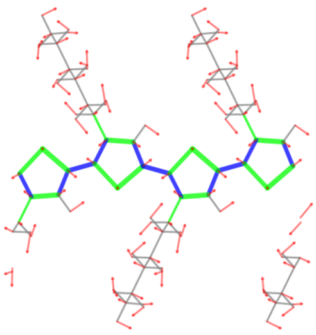
ν (cm^{-1})	1235	1217
I_{Raman} (10^3 Å^4 amu^{-1})	62	26
Irrep – mode	A_g – ECC ring + interring CC stretch; CS symm stretch	A – ECC ring + interring CC stretch + CC chain; CS stretch

Table 2. *Cont.*

	PT – 1D crystal	P3HT – 1D crystal
	Raman modes	**Raman and IR modes**
	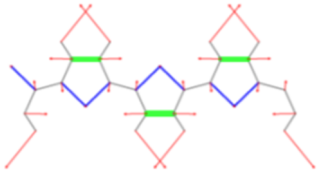	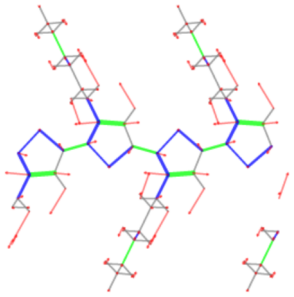
ν (cm^{-1})	1406	1407
I_{Raman} (10^3 Å^4 amu^{-1})	191	742
I_{IR} (km mol^{-1})	-	91
Irrep – mode	A_g ring C–C stretch; CH wag	A – CC stretch (ECC) + CC chain; CH wag
	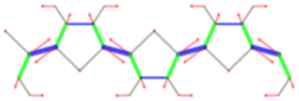	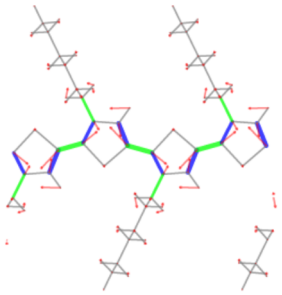
ν (cm^{-1})	1477	1467
I_{Raman} (10^3 Å^4 amu^{-1})	2281	1798
I_{IR} (km mol^{-1})	-	515
Irrep – mode	A_g collective ECC mode	A collective ECC mode

3.2. Modelling of TN Oligomers

In Table 3 and Figure 2, we compare the geometric parameters and vibrational spectra of TN oligomers of increasing length—from T4 to T45—and of the 1D crystal model, in order to highlight any trends that should converge to the one-dimensional crystal limit. The last two rows of Table 3 show how the structural parameters are affected by introducing the alkyl-substitution: more detailed comments will be presented in Section 4.

In our structural analysis, we focused on the central T2 unit of each oligothiophene model. The first observation is that the variations in the equilibrium CC bond lengths never exceed 0.002 Å. The calculated values are already stable from the T8 oligomer onward, with the central unit exhibiting the same geometry as the polymer. When we compare values obtained with different codes (i.e., Gaussian and CRYSTAL) using the same basis set, we observe similar trends for increasing oligomer length (i.e., number of T2 units). The same considerations also apply to the CS bond length, which appears to be independent of the oligomer size. However, the inter-ring CC bond lengths—R_{CC} (int-ring)—are systematically shorter in Gaussian compared to CRYSTAL. As described above (Methods), the forms of the Vosko-Wilk-Nusair (VWN) correlation functional employed in B3LYP [67] are different in Gaussian (VWN-III) and CRYSTAL (VWN-V). Our results highlight the sensitivity of the calculations to this choice, suggesting that the form of the VWN correlation functional may have a measurable impact in low-gap systems with highly delocalized electrons. This impact is even more significant when considering selected spectroscopic parameters. For this reason, we decided to analyse in parallel spectroscopic data obtained from B3LYP-V and B3LYP-III calculations.

Table 3. Equilibrium bond lengths of the central unit of TN oligomers and PT (described as a 1D crystal). Data were obtained from DFT geometry optimization performed with the CRYSTAL and Gaussian codes at the B3LYP-V/POB-TZVP and B3LYP-III/POB-TZVP levels, respectively. Structural parameters for P3HT and for 3HT8 are reported in the last two rows; asterisks (*) highlight the bonds located closer to the hexyl chain.

	R_{CC} (Ring) [Å]		$R_{C=C}$ [Å]		R_{CC} (Int-Ring) [Å]		R_{CS} [Å]	
	B3LYP V	**B3LYP III**	**B3LYP V**	**B3LYP III**	**B3LYP V**	**B3LYP III**	**B3LYP V**	**B3LYP III**
PT	1.408	-	1.374	-	1.434	-	1.775	-
T45	-	1.407	-	1.374	-	1.432	-	1.775
T22	1.408	1.407	1.374	1.374	1.434	1.432	1.775	1.775
T18	1.408	1.407	1.374	1.374	1.434	1.432	1.775	1.775
T14	1.408	1.407	1.374	1.374	1.434	1.432	1.775	1.775
T12	1.408	1.407	1.374	1.374	1.434	1.432	1.775	1.775
T8	1.408	1.407	1.374	1.374	1.434	1.432	1.775	1.775
T6	1.409	1.408	1.374	1.374	1.435	1.433	1.775	1.775
T4	1.411	1.410	1.372	1.373	1.436	1.434	1.775	1.775
P3HT	1.414	-	1.383(*)/1.374	-	1.439	-	1.782(*)/1.773	-
HT8	1.415	-	1.383(*)/1.374	-	1.439	-	1.781(*)/1.773	-

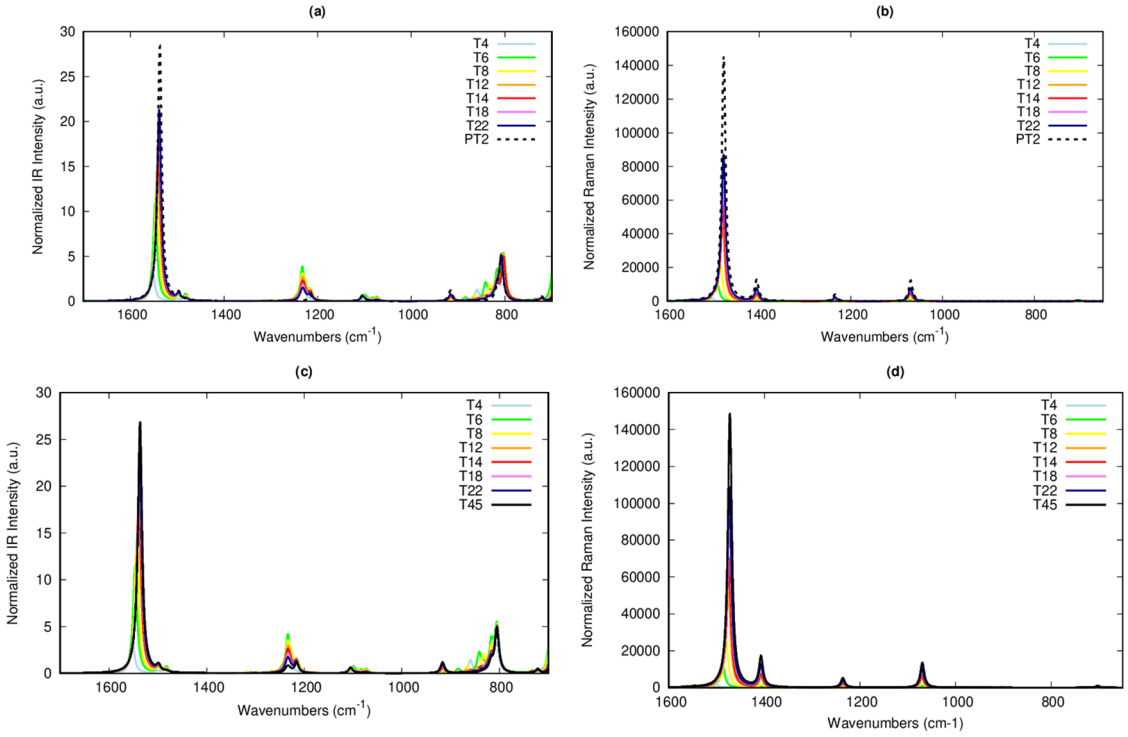

Figure 2. IR and Raman spectra of: TN oligomers obtained from DFT calculations using B3LYP-V/POB-TZV (CRYSTAL)—panels (**a**,**b**)—and the B3LYP-III/POB-TZVP (Gaussian code)—panels (**c**,**d**). The IR and Raman intensities are normalized with respect to the number of internal T2 units in the oligomer to enable comparison with the D crystal, whose translational unit is T2.

The analysis and comparison of the calculated spectra constitute the main objective of this investigation and allow us to highlight the effects of increasing the number of conjugated π-electrons on the spectroscopic response of systems composed of thiophene units. The vibrational spectral features of the oligomers are shown in Figures 2 and 3 and in Table S1 (Supplementary Material). A straightforward inspection of the spectral properties, supported by the analysis of the vibrational eigenvectors (Figure 4), shows that:

1. The IR and Raman spectra exhibit dominant transitions in the 1600–600 cm^{-1} region (Figure 2). The intense IR band of the oligomers appears close to the band of the 1D crystal which is assigned to the antisymmetric (*R*–) stretching of the C=C bonds in the thiophene ring (see Figures 2 and 3a). As expected, the vibrational eigenvectors of the oligomers correspond to a collective displacement pattern recognizable as *R*– (Figure 4)**.** The most intense Raman band of the oligomers shows a more pronounced frequency dispersion with increasing number of thiophene rings in the backbone. This band converges toward the frequency of the ECC

band of the 1D crystal as the oligomer length increases (Figure 3b), and the analysis of the oligomer eigenvectors reveals an evident ECC-like displacement pattern (Figure 4).

2. Figure 2 shows that, even after normalizing the oligomer intensities to the number of internal thiophene-ring pairs—i.e., excluding the two terminal rings (for TN, $I_{norm}=\frac{I}{(N-2)/2}$)—a non-negligible increase in the normalized intensity is still observed as *N* increases (i.e., the values do not reach convergence to the intensity of the corresponding vibrational transitions of the 1D crystal). This behaviour is highlighted in Figure 3c for the *R*– IR band and becomes particularly pronounced in the case of the ECC Raman band (Figure 3d).
3. In addition to the dominant bands discussed in point 1, the calculated spectra allow the identification of other significant bands, although weaker in intensity, which show a good correspondence between their peak frequencies and those of the analogous bands of the 1D crystal (Table S1). It is important to note that each IR/Raman band of the 1D crystal (selected based on its relative intensity and corresponding to one of the normal modes reported in Table 2) exhibits a clear counterpart in the spectrum of each oligomer. Table S1 provides a quantitative overview of the frequency and intensity trends of these bands and of their excellent frequency correlation with the corresponding bands of the 1D crystal. The analysis of the vibrational eigenvectors of the oligomers further confirms this clear correspondence of normal modes: in the oligomers, these modes are characterized by collective vibrational displacements in which all T2 units move in phase. Each of these modes can be directly related to the displacement pattern of the corresponding $\boldsymbol{q} = \mathbf{0}$ phonon of the 1D crystal, illustrated in Table 2 (see also Figure S1).
4. A careful analysis of the spectra of the shortest oligomers reveals the presence of bands that have no counterpart in the 1D crystal spectra. These bands are typically associated either with modes localized on the end units, or with collective modes corresponding to vibrations that are inactive in the 1D crystal, or with modes that can be described as phonons with wavevector $\boldsymbol{q} \neq \mathbf{0}$ (see, for example, the modes shown in Figure S2).

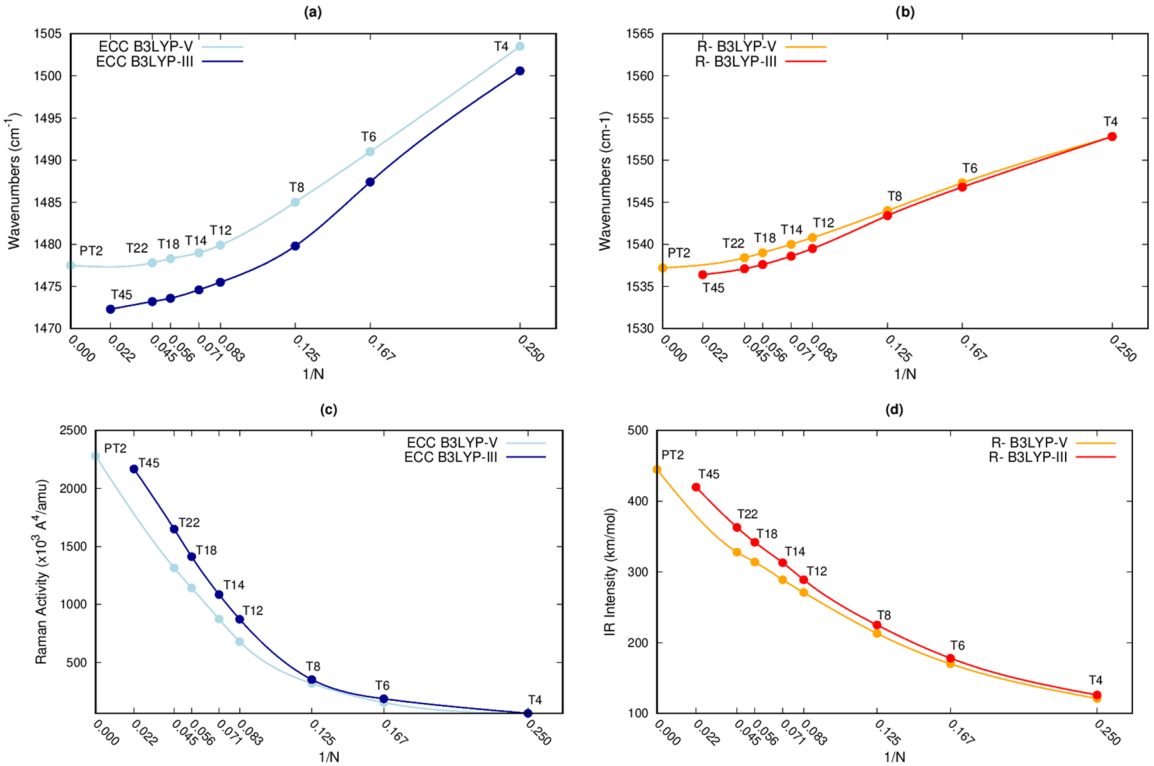

Figure 3. Plot of the vibrational wavenumber of the IR-active collective mode (*R*– band) and of the Raman-active collective ECC mode of TN oligomers and of the PT polymer described as a 1D crystal, as a function of 1/N (panels (**a**,**b**), respectively). The point 1/N = 0 corresponds to the ideal 1D crystal composed of an infinite number of thiophene units. Plot of the intensity of the *R*– band and of the Raman activity of the ECC band for TN oligomers and for the PT polymer described as a 1D crystal, as a function of 1/N (panels (**c**,**d**), respectively). The oligomer intensities are normalized to the number of internal thiophene units of the TN oligomer, $I_{norm} = I/[(N - 2)/2]$.

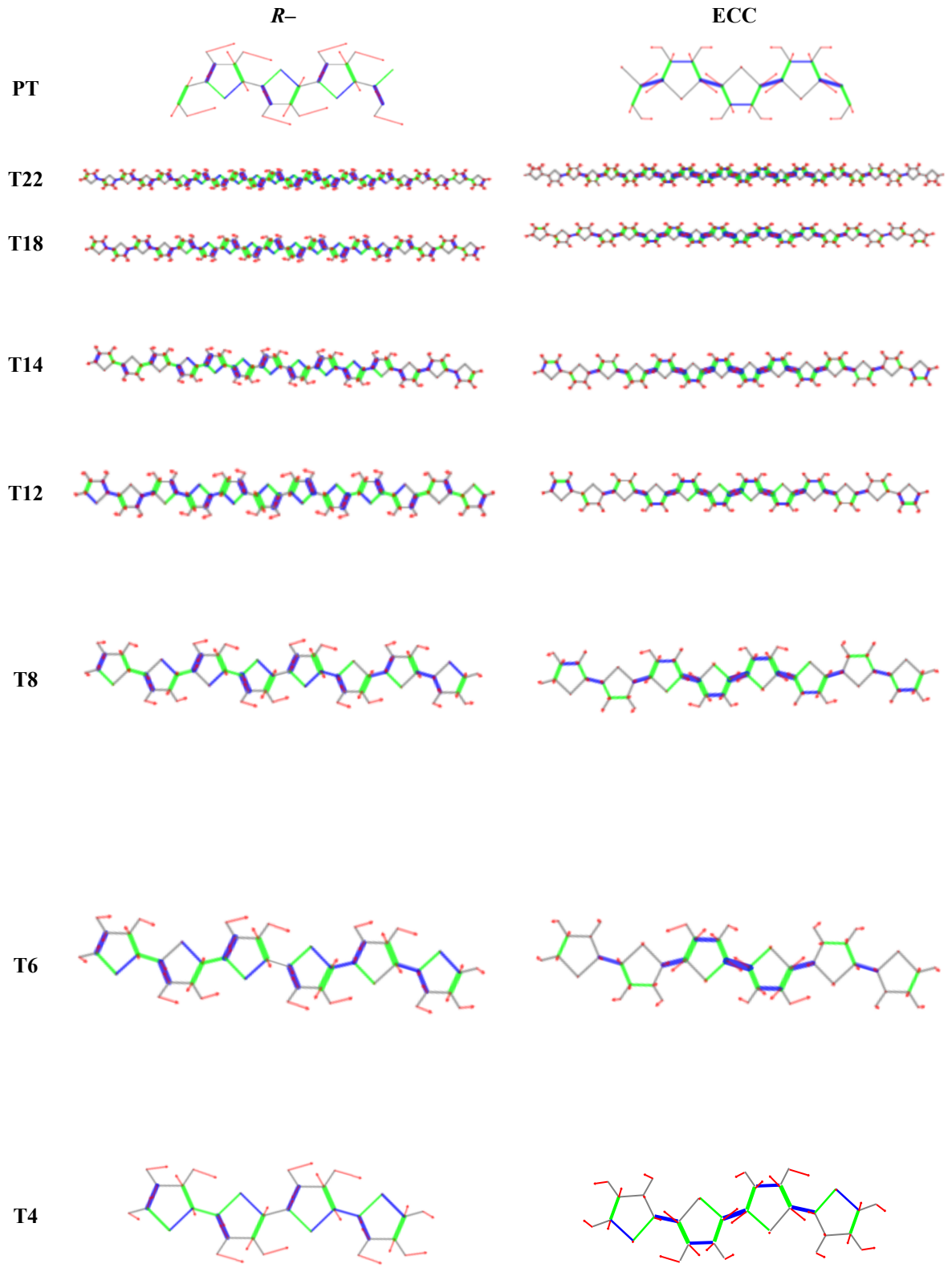

Figure 4. *Cont.*

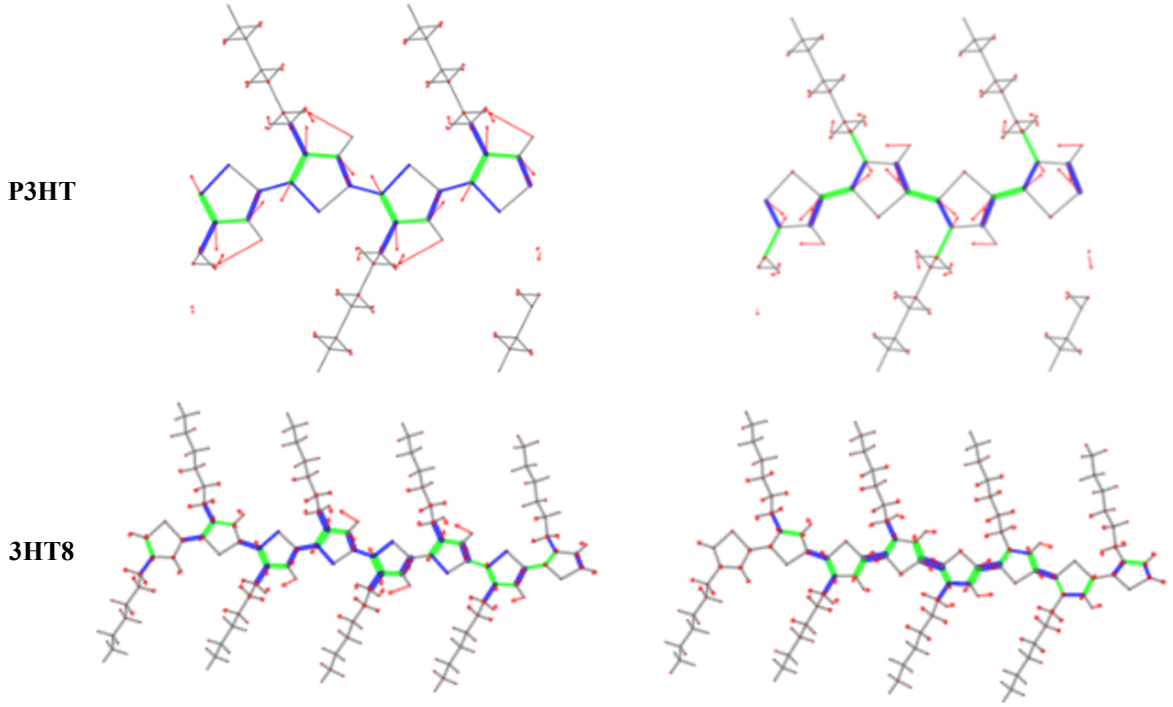

Figure 4. Vibrational eigenvectors of TN oligomers and 3HT8 assigned to the collective *R*– and ECC modes, and comparison with the eigenvectors of the corresponding $\boldsymbol{q} = \mathbf{0}$ modes of the 1D crystals (PT and P3HT). The reported eigenvectors correspond to calculations performed with the B3LYP-V/POB-TZV. Green and blue segments indicate bond stretching and contraction, respectively; segment thickness is proportional to the contribution of each bond deformation to the vibrational eigenvector. Red arrows represent the direction of atomic displacements within the normal mode.

Based on the modelling of the vibrational spectra of the TN molecules performed with the B3LYP-V functional (CRYSTAL) (Figure 2a,b), we can conclude that the IR and Raman spectral patterns of planar oligomers are very similar to those of the polymer modelled as a 1D crystal, at least starting from the T6 oligomer. Quantitatively, most of the band frequencies remain nearly constant with increasing N and match the values obtained for the polymer (Table S1). However, this trend does not apply to the two modes that correspond to the most intense IR and Raman bands. In fact, we observe a significant frequency dispersion for the *R*– IR transition ($\Delta\nu = 16$ cm^{-1} from T4 to PT, reduced to $\Delta\nu = 10$ cm^{-1} from T6 to PT). We also observe significant dispersion for the ECC mode, whose band overwhelmingly dominates the Raman spectrum of all oligomers and exhibits the largest frequency dispersion ($\Delta\nu = 26$ cm^{-1} from T4 to PT, reduced to $\Delta\nu = 14$ cm^{-1} from T6 to PT). Only above T8 does the plateau start to be reached. Considering the positions of the *R*– and ECC bands, the T12 oligomer provides an excellent approximation to PT, with deviations reaching 4 cm^{-1} and 3 cm^{-1}, respectively.

The trend in B3LYP-V -computed intensities exhibits a markedly different behaviour. Although the relative intensities of the peaks are well reproduced, the absolute intensities are significantly underestimated by the oligomer models. In particular, the Raman activity of the ECC mode steadily increases super-linearly with oligomer length: the ECC intensity of T4, normalized to the number of T2 units, is roughly 30 times smaller than that of the polymer, and it does not show any indication of reaching a plateau along the series from T4 to T22. Notably, the Raman intensity of PT is nearly twice that of T22 and increases by a factor of 26 from T4 to PT (Figure 3c). The effect is less pronounced for the IR spectrum (using the same normalization): the *R*– mode of PT is 1.4 times more intense than that of T22, and PT exceeds T4 by a factor of 10 (Figure 3d).

The same observations apply to the oligomer spectra computed with the B3LYP-III functional (Gaussian). In this case, we consider T45 as the limiting case, which we assume to be an excellent approximation to the infinite model. Despite the systematically lower frequencies obtained with B3LYP-III relative to B3LYP-V, the overall trends are essentially parallel, both considering the *R*– and the ECC mode (see Table S1 and Figure 3a,b). It is noteworthy that, among the normal modes, the ECC mode computed with B3LYP-III exhibits the largest deviations, for both frequencies and intensities, relative to the data obtained with the B3LYP-V functional. These differences clearly stem from the strong sensitivity of ECC to electron–phonon coupling and thus to subtle variations in the description of the π-electron structure arising from slight differences in the correlation potential between B3LYP-V and B3LYP-III.

All observations of the trends in frequency and intensity can be rationalized by noting that the increased π-electron delocalization, which is expected as the length of the TN oligomer backbone increases, affects vibrational dynamics. The effect is mostly evident for the CC stretching modes, and it is particularly pronounced for the ECC mode, for which the presence of long-range interactions results in the well-known softening of the frequency [70,71,74,75].

Vibrational intensities are known to be highly sensitive to the degree of π-electron conjugation [35,62,67]. An extended π-system enhances the molecular polarizability and, consequently, the Raman polarizability associated with the ECC mode. IR intensities in conjugated systems can also be very large when significant charge fluxes occur [36,75]. This phenomenon is less widely recognized because it pertains to π-polarized systems and therefore does not arise when the vibrating bonds are non-polar or centrosymmetric. It has been demonstrated that breaking inversion symmetry can lead to exceptional IR-intensity enhancement, for example, in push–pull polyenes substituted at the two termini with an acceptor and a donor group respectively [75], or upon doping of conjugated polymers [36,70]. It is evident that heteroaromatic rings with polarized C=C bonds may display intense IR bands due to substantial charge flux associated with π-electron delocalization.

In conclusion, the T12 oligomer can be proposed as an adequate structural and spectroscopic model of the polymer. However, while the Raman spectrum is expected to reproduce the relative intensities well, the absolute intensities will be significantly underestimated. The fact that a planar T12 oligomer provides a suitable representation of the polymer in its regular planar conformation suggests that T12 molecular models with irregular non-planar conformations can satisfactorily describe a polymer containing structural defects. In other words, this oligomer could effectively mimic the behaviour of polymer solutions or amorphous phases. Conversely, we have verified that the 1D model—whose computational cost is dramatically lower, as the polymeric repeating unit is reduced from twelve to just two thiophene units—can also be suitable for describing the spectroscopic behaviour of partially distorted finite-size systems, provided that their conjugation length is comparable to that of an oligomer containing approximately ten coplanar thiophene rings.

4. Poly(3-Hexylthiophene) as a 1D Crystal and the 3HT8 Oligomer

To support the structural characterization of one of the most widely studied and technologically relevant conducting polymers, we extended our analysis to include the structure and vibrational spectra of P3HT. This polymer exhibits crystalline domains—both in the neutral and doped states—with degrees of crystallinity and morphologies that strongly depend on the preparation protocol of the solid material, which can be processed either as thin films or as fibers [11–13,16–18]. In the crystalline phase, the polymer adopts a conformation in which the thiophene rings are either fully coplanar or display slight deviations from planarity. On this basis, we modelled the polymer chain as a one-dimensional crystal, with a translational unit composed of two 3-hexylthiophene (HT) moieties. A screw axis with rotation $\theta = \pi$ relates the two HT groups, so that the polymer line group is isomorphic to the point group C_2, and the minimal asymmetric unit consists of a single HT moiety. In this configuration, the alkyl side chain adopts an all-trans conformation and is attached to the thiophene ring with a torsional angle $\tau = 90°$ about the C–C bond linking the ring carbon to the first CH_2 unit of the hexyl chain, while the hexyl chain axis is tilted by $\Theta = 140°$ with respect to the backbone axis. This geometry had already been identified in a previous theoretical study [43] and is consistent with crystallographic data for the most stable crystalline phase of P3HT and related oligomers [11,14,15]. The structural parameters obtained after optimization of the 1D crystal geometry are reported in Table 3, allowing direct comparison with those of unsubstituted polythiophene.

The introduction of the hexyl group produces mainly the following structural effects on the 1D crystal model of P3HT—hereafter referred to as P3HT:

(i) A significant elongation of the C–C bonds: both the quasi-single C–C bond within the thiophene ring and the inter-ring C–C bond in P3HT are longer than in PT, with $\Delta R \approx 0.05$ Å. Based on this observation, the P3HT backbone may be described as more aromatic than that of PT.

(ii) A pronounced asymmetry between the two C=C bonds of the ring: the C=C bond adjacent to the substituent elongates by $\Delta R \approx 0.05$ Å, whereas the other C=C bond has essentially the same length as in PT. This loss of local C_{2v} symmetry of the ring is expected to strongly affect the vibrational dynamics.

Figure 5 reports the Raman and IR spectra of P3HT, which can be compared with the spectra calculated for PT in Figure 1. The first aspect to underline is the excellent agreement between the computed IR and Raman spectra of P3HT (Figure 5a,b)—modelled as a 1D crystal—and the corresponding experimental spectra recorded from solid P3HT samples (Figure 5c,d). Table 2 displays the eigenvectors of selected normal modes corresponding to IR or Raman-active bands of P3HT with significant intensity, together with the corresponding PT modes, showing a close correspondence in atomic displacement patterns and wavenumbers.

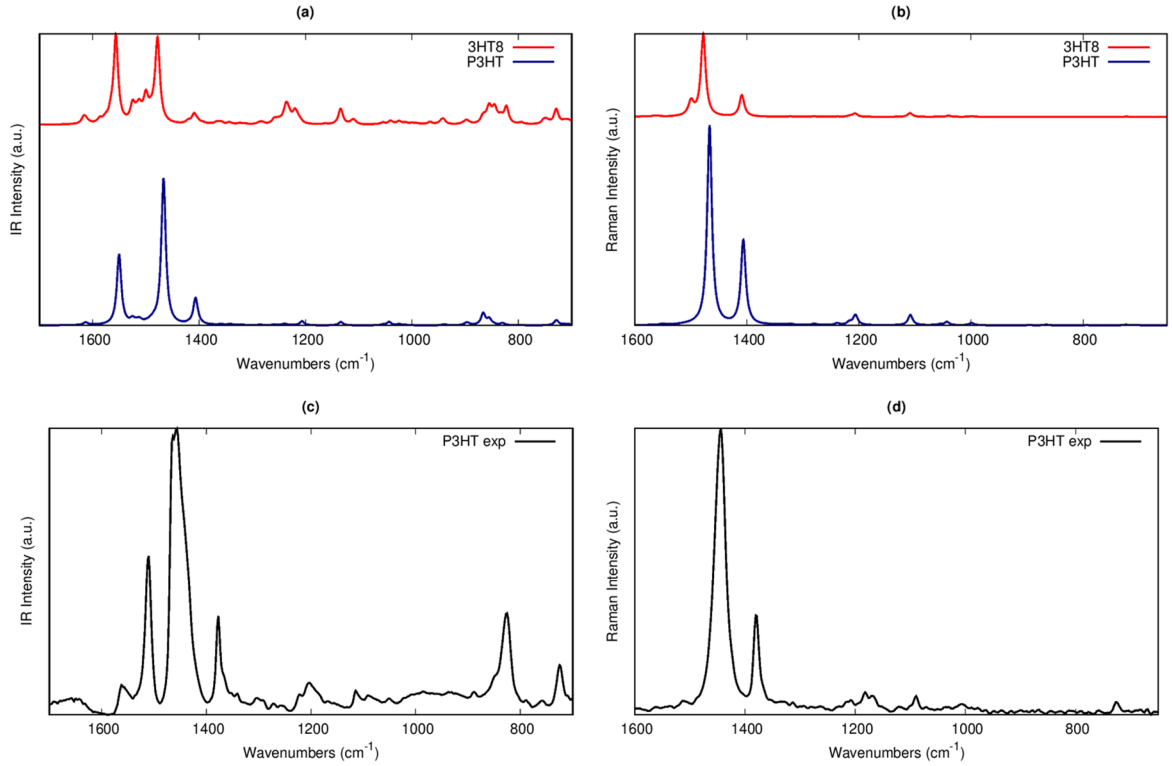

Figure 5. B3LYP-V/POB-TZVP calculated and experimental IR and Raman spectra of P3HT in panels (**a**,**b**), and in panels (**c**, **d**), respectively. The upper panels also show the vibrational spectra of the 3HT8 oligomer. Experimental details are reported in ref. [51].

The IR spectrum of P3HT shows marked differences with respect to that of PT. Apart from the obvious appearance of intense stretching bands of the CH_2 and CH_3 groups of the hexyl chain (computed between 3000 and 3100 cm^{-1}), the region below 1600 cm^{-1} becomes substantially more complex. The most evident effect—directly related to the symmetry reduction—is the IR activation of the two strongest Raman transitions (ν = 1407 cm^{-1} and ν = 1467 cm^{-1}, respectively). The position and especially the strong Raman intensity of the 1467 cm^{-1} band support its assignment to the collective ECC mode, as confirmed by inspection of the vibrational eigenvector (Table 2). Notably, in the IR spectrum of P3HT, the ECC band becomes significantly more intense than the antisymmetric *R*– stretching band (ν = 1550 cm^{-1}). This behaviour reflects strong charge-flow contributions along the polymer backbone induced by the ECC vibration that becomes IR-allowed due to the loss of inversion symmetry and the involvement of polarized C–C bonds.

The Raman region below 1350 cm^{-1} is complicated by the coupling between backbone vibrations and the CH_2 bending modes of the hexyl substituents. This mixing makes it difficult to establish a one-to-one correspondence between the modes of P3HT and those of unsubstituted PT. Table 2 reports a selection of P3HT eigenvectors that exhibit a large projection onto the corresponding PT modes. However—as illustrated in Figure S3—several P3HT modes may correspond to a single PT mode while still retaining similar thiophene-ring displacement patterns. This explains why the paired modes listed in Table 2 can sometimes show markedly different Raman intensities in PT and P3HT.

This observation mostly concerns the two dominant Raman bands at 1407 and 1467 cm^{-1}, which correlate with the PT bands at 1406 and 1477 cm^{-1}. In particular, the 1407 cm^{-1} band is approximately four times more intense than the corresponding band of PT. The different relative intensity of these two Raman features can be rationalized by a detailed comparison of the eigenvectors in Table 2, which reveal important differences:

(i) The stretching of the C–C bond linking the hexyl chain to the thiophene ring is strongly involved in both P3HT modes, vibrating out of phase and in phase, respectively, with the adjacent ring C=C bond.

(ii) Both P3HT modes include a significant contribution from inter-ring C–C stretching**,** whereas in PT only the higher-frequency, more intense mode involves substantial inter-ring stretching.

(iii) The 1467 cm^{-1} mode of P3HT exhibits negligible contribution from the quasi-single C–C ring bond**,** whereas the corresponding PT mode at 1477 cm^{-1} clearly involves this internal coordinate.

Observations (ii) and (iii) demonstrate that the ECC coordinate is involved to different extents in the two polymers: the 1406 cm^{-1} mode of P3HT possesses a stronger ECC character compared to the corresponding mode

of PT, which fully accounts for the enhanced intensity of the 1406 cm^{-1} band in P3HT. It is also noteworthy that the most intense ECC mode occurs at a lower frequency in P3HT than in PT; this might be misinterpreted as evidence of enhanced π-electron conjugation along the backbone, contradicting the structural findings. Instead, the frequency shift is more reasonably attributed to differences in dynamic coupling, in particular the participation of the side-chain C–C stretching in the collective vibration.

In a previous work [36], the 3HT8 oligomer was proposed as a molecular model of P3HT, based on the idea that it provides a good compromise between computational cost and the quality of the predicted spectroscopic response of the polymer. On the one hand, a sufficiently extended backbone is required to properly describe effects that depend on the degree of π-electron delocalization; on the other hand, it is necessary to realistically describe the alkyl chains, whose vibrations modify the spectral pattern both through dynamic couplings—in particular between the CC-stretching modes of the backbone and the bond by which the hexyl group is attached to the thiophene ring—and through intense vibrations, e.g., CH-stretching modes localized on the alkyl chain.

By directly comparing the results from the calculation of the 1D infinite P3HT crystal model with those from the calculation on 3HT8, performed at the same level of theory, it is now possible to highlight the strengths and limitations of the molecular model. Figure 5, panels a and b, shows the direct comparison between the calculated spectra for P3HT and 3HT8. Several observations are immediate:

1. The IR and Raman spectral patterns of P3HT (as a 1D crystal) are reproduced very well by the molecular model: in particular, all the intense transitions of P3HT correspond (both in frequency and in vibrational mode description) to intense transitions of the oligomer.
2. The spectra of 3HT8—especially the IR spectrum—contain a larger number of peaks, due to the presence of modes localized at the terminal regions and to the activation of modes corresponding to phonons with wavevector $\boldsymbol{q} \neq \mathbf{0}$ in the polymer. This latter phenomenon is responsible for the peak appearing near the ECC band, calculated at about 1500 cm^{-1}, which arises from the convolution of bands associated with different ECC-like transitions.
3. The vibrational band intensities of the oligomer are, overall, significantly weaker than those of the polymer. In fact, although Figure 5 reports the 3HT8 spectra without the normalization required for proper comparison with the polymer—whose intensities refer to a translational unit of two HT rings—both the IR and Raman spectra of the oligomer appear significantly weaker. Table S2 allows for a quantitative comparison of the intensities of selected bands (IR and Raman) for the two models: it is interesting to note that both IR and Raman modes with significant ECC character show the largest discrepancies in intensity. For this reason, the relative intensity of the two strong IR-active bands assigned to the *R*– mode and to the ECC mode (see sketches of eigenvectors, Figure 4) differs between the IR spectra of 3HT8 and P3HT. This feature can be explained by a different charge-flux contribution associated with the ECC mode, which becomes increasingly relevant as the π-system extension increases.
4. The same phenomenon can be observed when considering the full IR spectrum (Figure S4), including the region around 3000 cm^{-1}, which contains dominant contributions from CH_2-stretching vibrations of the alkyl chains: while in the oligomer the CH-stretching bands display overall higher intensity than the CC-stretching bands (ECC, *R*–), in the P3HT – 1D crystal the latter dominate the spectrum.

Comparison with the experimental solid-state spectrum of P3HT suggests that the 1D crystal model reproduces the overall intensity pattern below 1600 cm^{-1} more accurately than the oligomer model (Figure 5). However, the oligomeric model can still be considered satisfactory for investigating the spectroscopic properties of the polymer, provided that the limitations of the molecular model are carefully taken into account—namely, by disregarding modes mainly involving terminal groups and those activated by the relaxation of translational symmetry. Moreover, the systematic underestimation of vibrational intensities provided by the molecular model should be carefully considered. In this respect, we cannot overlook the well-known issues related to the calculation of absolute intensities of conjugated systems: DFT methods are believed to overemphasize delocalization effects [75,76], which could explain why the CH-stretching region dominates the experimental IR spectrum of the polymer (Figure S4) while the calculation for the ideally infinite chain indicates that the ECC band is the strongest one. Interestingly, the prediction for 3HT8 shows an intensity pattern that more closely matches the experiment, possibly due to electron confinement arising from its finite size.

5. Conclusions

We critically compared the intrachain structural and spectroscopic properties obtained by DFT calculations on thiophene oligomers (TN and 3HT8) and polymers (PT, P3HT) described as ideal one-dimensional (1D) crystals. This analysis confirmed that vibrational modes involving CC stretching of the ring and of the inter-ring bond are

sensitive to the conjugation length. Such an effect is due to electron-phonon coupling, and is particularly pronounced for vibrations whose atomic displacements have a non-zero projection along the effective conjugation coordinate.

The results for the TN oligomers show that the spectroscopic features of the infinite model (vibrational frequencies and relative IR and Raman intensities) are already well approximated starting at N = 8, and are excellently reproduced by T12. Notably, the frequency of the most intense Raman-active mode (ECC mode) converges to the limiting value of the 1D-crystal polymer for increasing oligomer length.

The behaviour of the vibrational intensities with increasing molecular size is peculiar. In fact, for the range of molecular sizes explored in this work, the intensity of the strong vibrational transitions—particularly the most intense Raman-active modes—varies in a more-than-linear fashion with N. It is well known that the presence of an extended, delocalized π-electron system can strongly affect both IR transition dipoles and Raman polarizability tensors [75]. These aspects must therefore be considered when discussing transition intensities calculated with oligomeric models.

The relationships established here between the spectroscopic response of the 1D-crystal model and that of oligomers enable the critical use of both types of models in the interpretation of experimental data. The infinite-chain model, thanks to translational symmetry, drastically reduces computational cost and can be extremely advantageous for describing the solid-state properties of thiophene polymers with more complex structural units, such as polythiophenes with grafted side chains (P3HT) or doped polythiophenes in the crystalline phase. Besides, the description of disordered systems, such as polythiophenes in solution or in the amorphous phase, can be addressed using sufficiently extended molecular models.

The main critical issue highlighted by this study is that the computed absolute Raman and IR intensities do not converge even for large oligomers (up to T22), suggesting that finite-size models are inherently limited in their ability to predict the absolute spectroscopic response of the polymer. Anyway, a limitation of the 1D model is the absence of three-dimensional interchain interactions (packing effects), which warrants further investigation in future work.

The present work focuses exclusively on the pristine (neutral) states of PT and P3HT, but it provides a solid foundation for investigating their doped states. We believe that this detailed investigation offers a useful starting point for developing theoretical models that enable increasingly refined and well-grounded interpretations of the many spectroscopic signatures of polythiophenes, across different phases (solution, crystalline/amorphous solid) and doping-induced states. The spectroscopy of these systems—and, more generally, of polymeric semiconductors and conductors—has long been an essential tool for establishing structure–property relationships; a rigorous theoretical approach can significantly support empirical evidence and correlations that remain only partially understood.

In this context, this study illustrates a methodology that can be readily extended to new π-conjugated materials arising from state-of-the-art chemical synthesis approaches, specifically designed for technologically relevant applications [19–25]. In this scenario, the comparison between the properties calculated for small oligomers and for the 1D crystal is expected to clarify the advantages and limitations of the two approaches. Notably, at least for ordered phases, calculations performed using periodic boundary conditions allow the investigation of systems with large and potentially complex monomeric units, including copolymers and chemically doped polymers, such as the ones used in organic photovoltaic or thermoelectric devices. Moreover, if the unit cell of the 1D crystal is of moderate size, the transition to 3D crystal calculations is straightforward and enables the study of packing effects or specific interchain interactions on the geometric and electronic structure of the material.

In conclusion, the modelling strategies presented in this work pave the way for the rationalization of the structure-properties relationship of new-generation conducting polymers through their vibrational response, even when they possess a more complicated chemical structure than P3HT.

Supplementary Materials

The additional data and information can be downloaded at: https://media.sciltp.com/articles/others/26040716 55225503/PS-25120076-SI.pdf. Table S1: Wavenumbers and intensities of the most prominent IR and Raman bands of TN oligomers of polythiophene (PT). Figure S1: Comparison of the $\boldsymbol{q} = \mathbf{0}$ vibrational eigenvectors associated with the strongest IR and Raman bands of PT as 1D crystal—with those of the corresponding modes of T12 (DFT B3LYP-V/POB-TZVP calculations, CRYSTAL CODE). Figure S2: Examples of end modes and modes associated with $\boldsymbol{q} \neq \mathbf{0}$ phonons of the 1D crystal, illustrated through vibrational eigenvectors of T6 and T4, calculated at the DFT B3LYP-V/POB-TZVP level (CRYSTAL code). For each selected mode, the calculated wavenumber and IR or Raman intensity are reported. Table S2: Wavenumbers and intensities of the most prominent IR and Raman bands of P3HT (1D crystal) and its 3HT8 oligomer. The values are obtained from DFT

calculations (B3LYP-V/POB-TZVP) with the CRYSTAL code. Figure S3: Raman modes of PT showing features shared with multiple P3HT modes (see manuscript). Sketches of the vibrational eigenvectors of PT and P3HT treated as 1D crystals. Figure S4**:** Calculated IR and Raman spectra for the 1D crystal model of P3HT (panels (**a**,**b**)) and for the 3HT8 molecule (panels (**c**,**d**)). Calculations were performed using the CRYSTAL code at DFT B3LYP-V/POB-TZVP level. Panels (**e**,**f**) report the experimental IR and Raman spectra of a solid sample of P3HT.

Author Contributions

C.S.: writing—original draft preparation, conceptualization, investigation, data curation, reviewing and editing; M.T.: conceptualization, software, methodology, validation, reviewing and editing; D.R.G.: conceptualization, methodology, validation, reviewing and editing; C.C.: writing—original draft preparation; investigation; conceptualization, supervision. All authors have read and agreed to the published version of the manuscript.

Institutional Review Board Statement

Not applicable.

Informed Consent Statement

Not applicable.

Data Availability Statement

The data presented in this study are (i) available in the article or the Supplementary Materials or (ii) available upon request from the corresponding author.

Acknowledgments

The authors acknowledge CINECA for providing computational time and data storage through the Italian SuperComputing Resource Allocation (ISCRA) initiative, project code IsCc5—HP10CFKOVP.

Conflicts of Interest

The authors declare no conflict of interest.

Use of AI and AI-Assisted Technologies

No AI tools were utilized for this paper.

References

1. Skotheim, T.A.; Elsenbaumer, R.L.; Reynolds, J.R. (Eds.) *Handbook of Conducting Polymers*, 2nd ed.; Marcel Dekker: New York, NY, USA, 1988.
2. Perepichka, J.F.; Perepichka, D.F. (Eds.) *Handbook of Thiophene Based Materials*; Wiley: Chichester, UK, 2009.
3. Roth, S.; Carrol, D. *One-Dimensional Metals*; Wiley-VCH: Weinheim, Germany, 2004.
4. Brédas, J.L.; Silbey, R. *Conjugated Polymers*; Springer: Dordrecht, The Netherlands, 1991.
5. Pope, M.; Swenberg, C.E. *Electronic Processes in Organic Crystals and Polymers*; Oxford University Press: Oxford, UK, 1999.
6. Kroon, R.; Mengistie, D.A.; Kiefer, D.; et al. Thermoelectric Plastics: From Design to Synthesis, Processing and Structure–Property Relationships. *Chem. Soc. Rev.* **2016**, *45*, 6147–6164.
7. Kim, T.; Yang, S.J.; Sung, S.J.; et al. Highly Reproducible Thermocontrolled Electrospun Fiber Based Organic Photovoltaic Devices. *ACS Appl. Mater. Interfaces* **2015**, *7*, 4481–4487.
8. Bharti, M.; Singh, A.; Samanta, S.; et al. Conductive Polymers for Thermoelectric Power Generation. *Prog. Mater. Sci.* **2018**, *93*, 270–310.
9. Ludwigs, S. (Ed.) *P3HT Revisited—From Molecular Scale to Solar Cell Devices*; Springer: Berlin, Germany, 2014; Volume 256.
10. Sumdani, G.M.; Islam, R.M.; Yahaya, N.A.A.; et al. Recent Advancements in Synthesis, Properties, and Applications of Conductive Polymers for Electrochemical Energy Storage Devices: A Review. *Polym. Eng. Sci.* **2022**, *62*, 269–303.
11. Tashiro, K.; Kobayashi, M.; Kawai, T.; et al. Crystal Structural Change in Poly(3-Alkyl Thiophene)s Induced by Iodine Doping as Studied by an Organized Combination of X-ray Diffraction, Infrared/Raman Spectroscopy and Computer Simulation Techniques. *Polymer* **1997**, *38*, 2867–2879.

12. Brinkmann, M. Structure and Morphology Control in Thin Films of Regioregular Poly(3-hexylthiophene). *J. Polym. Sci. B* **2011**, *49*, 1218–1233.
13. Rahimi, K.; Botiz, I.; Stingelin, N.; et al. Controllable Processes for Generating Large Single Crystals of Poly(3-hexylthiophene). *Angew. Chem. Int. Ed.* **2012**, *51*, 11131–11135.
14. Dudenko, D.; Kiersnowski, A.; Shu, J.; et al. A Strategy for Revealing the Packing in Semicrystalline p-Conjugated Polymers: Crystal Structure of Bulk Poly-3-hexyl-thiophene (P3HT). *Angew. Chem. Int. Ed*. **2012**, *51*, 11068–11072.
15. Kayunkid, N.; Uttiya, S.; Brinkmann, M. Structural Model of Regioregular Poly(3-hexylthiophene) Obtained by Electron Diffraction Analysis. *Macromolecules* **2010**, *43*, 4961–4967.
16. Hamidi-Sakr, A.; Biniek, L.; Bantignies, J.-L.; et al. A Versatile Method to Fabricate Highly In-plane Aligned Conducting Polymer Films with Anisotropic Charge Transport and Thermoelectric Properties: The Key Role of Alkyl Side Chain Layers on the Doping Mechanism. *Adv. Funct. Mater.* **2017**, *27*, 1700173.
17. Lee, S.; Moon, G.D.; Jeong, U. Continuous Production of Uniform Poly(3-hexylthiophene) (P3HT) Nanofibers by Electrospinning and Their Electrical Properties. *J. Mater. Chem.* **2009**, *19*, 743–748.
18. Chen, J.Y.; Kuo, C.C.; Lai, C.S.; et al. Manipulation on the Morphology and Electrical Properties of Aligned Electrospun Nanofibers of Poly(3-hexylthiophene) for Field-Effect Transistor Applications. *Macromolecules* **2011**, *44*, 2883–2892.
19. Meng, B.; Liu, J.; Wang, L. Recent Development of n-Type Thermoelectric Materials Based on Conjugated Polymers. *Nano Mat. Sci.* **2021**, *3*, 113–123.
20. Liu, X.; Yan, Y.; Zhang, Q.; et al. n-Type D-A Conjugated Polymers: Relationship Between Microstructure and Electrical/Mechanical Performance. *Chem. Res. Chin. Univ.* **2021**, *37*, 1019–1030.
21. Du, C.H.; Xu, Y.H.; Li, H.; et al. Tough Hydrogen Bonding Crosslinked Poly(3-fluorothiophene) Network Via Electrosynthesis for High-Performance Electrochromic Supercapacitors. *Chin. J. Polym. Sci.* **2024**, *42*, 1749–1757.
22. Wu, Z.; Zhao, Q.; Luo, X.; et al. Low-Cost Fabrication of High-Performance Fluorinated Polythiophene-Based Vis−NIR Electrochromic Devices Toward Deformable Display and Camouflage. *Chem. Mater.* **2022**, *34*, 9923−9933.
23. Sugiyasu, K.; Honsho, Y.; Harrison, R.M.; et al. A Self-Threading Polythiophene: Defect-Free Insulated Molecular Wires Endowed with Long Effective Conjugation Length. *J. Am. Chem. Soc.* **2010**, *132*, 14754−14756.
24. Ouchi, Y.; Sugiyasu, K.; Ogi, S.; et al. Synthesis of Self-Threading Bithiophenes and Their Structure-Property Relationships Regarding Cyclic Side-Chains with Atomic Precision. *Chem. Asian J.* **2012**, *7*, 75−84.
25. Du, C.; Cheng, X.; Zhang, G.; et al. Molecular Bonding Engineering Enables Ultra-Stable Electrochromic Energy Storage in Flexible PEDOT Devices. *Adv. Mater.* **2025**, e16740. https://doi.org/10.1002/adma.202516740
26. Zbinden, R. *Infrared Spectroscopy of High Polymers*; Academic Press: New York, NY, USA, 1964.
27. Painter, P.C.; Coleman, M.M.; Koening, J.L. *The Theory of Vibrational Spectroscopy and Its Application to Polymeric Materials*; Wiley: Chichester, UK, 1982.
28. Zerbi, G. Molecular Vibrations of High Polymers. In *Applied Spectroscopy Reviews*, 2nd ed.; Brame, A.D., Ed.; Dekker: New York, NY, USA, 1969; Volume 2, p. 193.
29. Zerbi, G. Vibrational Spectroscopy of Very Large Molecules. In *Advances in Infrared and Raman Spectroscopy*; Clark, R.J.H., Hester, R.E., Eds.; Heyden: London, UK, 1984; Volume 11, p. 301.
30. Zerbi, G. *Modern Polymer Spectroscopy*; Wiley-VCH: New York, NY, USA, 1999; p. 113.
31. Zerbi, G. *Vibrational Spectroscopy of Polymers*; Everall, N.J., Chalmers, J.M., Griffith, P.R., Eds.; Wiley: Chichester, UK, 2007; p. 487.
32. Müllen, K.; Wegner, G. *Electronic Materials: The Oligomer Approach*; Wiley-VCH: Weinheim, Germany, 1998.
33. Zerbi, G.; Chierichetti, B.; Ingänas, O. Vibrational Spectra of Oligothiophenes as Model of Polythiophenes. *J. Chem. Phys.* **1991**, *94*, 4637–4645.
34. Zerbi, G.; Chierichetti, B.; Ingänas, O. Thermochromism in Polyalkylthiophenes: Molecular Aspects from Vibrational Spectroscopy. *J. Chem. Phys.* **1991**, *94*, 4646–4658.
35. Agosti, E.; Rivola, M.; Hernandez, V.; et al. Electronic and Dynamical Effects from the Unusual Features of the Raman Spectra of Oligo and Polythiophenes. *Synth. Met.* **1999**, *100*, 101–112.
36. Saporiti, C.; Brambilla, L.; Fazzi, D.; et al. Insights into the Structural and Vibrational Properties of Polaron in Doped Poly(3-alkyl-thiophene), P3HT. *J. Phys. Chem. C.* **2024**, *128*, 5189–5205.
37. Anderson, M.; Ramanan, C.; Fontanesi, C.; et al. Displacement of Polarons by Vibrational Modes in Doped Conjugated Polymers. *Phys. Rev. Mater.* **2017**, *1*, 055604.
38. Yin, J.; Wang, Z.; Fazzi, D.; et al. First-principles Study of the Nuclear Dynamics of Doped Conjugated Polymers. *J. Phys. Chem. C* **2016**, *120*, 1994–2001.
39. Wang, S.; Fazzi, D.; Puttisong, Y.; et al. Effect of Backbone Regiochemistry on Conductivity, Charge Density, and Polaron Structure of n-Doped Donor–Acceptor Polymers. *Chem. Mater.* **2019**, *31*, 3395–3406.
40. Furukawa, Y.; Akimoto, M.; Harada, I. Vibrational Key Bands and Electrical Conductivity of Polythiophene. *Synth. Met.* **1987**, *18*, 151–156.

41. Cao, Y.; Renyuan, Q. IR and Raman Studies of Polythiophene Prepared by Electrochemical Polymerization. *Solid State Commun.* **1985**, *54*, 211–213.
42. Louarn, G.; Trznadel, M.; Buisson, J.P.; et al. Raman Spectroscopic Studies of Regioregular Poly(3-alkylthiophenes). *J. Phys. Chem.* **1996**, *100*, 12532–12539.
43. Brambilla, L.; Tommasini, M.; Botiz, I.; et al. Regio-Regular Oligo and Poly(3-HexylThiophene): Precise Structural Markers from the Vibrational Spectra of Oligomer Single Crystals. *Macromolecules* **2014**, *47*, 6730–6739.
44. Brambilla, L.; Ferrón, C.C.; Tommasini, M.; et al. Infrared and Multi-Wavelength Raman Spectroscopy of Regio-regular P3HT and Its Deutero Derivatives. *J. Raman Spectrosc.* **2018**, *49*, 569–580.
45. Brambilla, L.; Kim, J.-S.; Kim, B.J.; et al. Poly(3-hexylthiophene-2.5-diyl): Evidence of Different Polymer Chain Conformations in the Solid State from a Combined Study of Regioregularity Control and Raman Spectroscopy. *J. Mol. Struct.* **2020**, *1221*, 128882.
46. Scholes, D.T.; Yee, P.Y.; Lindemuth, J.R.; et al. The Effects of Crystallinity on Charge Transport and the Structure of Sequentially Processed F4TCNQ-Doped Conjugated Polymer Films. *Adv. Funct. Mater.* **2017**, *27*, 1702654.
47. Stanfield, D.A.; Wu, Y.; Tolbert, S.H.; et al. Controlling the Formation of Charge Transfer Complexes in Chemically Doped Semiconducting Polymers. *Chem. Mater.* **2021**, *33*, 2343–2356.
48. Stanfield, D.A.; Mehmedović, Z.; Schwartz, B.J. Vibrational Stark Effect Mapping of Polaron Delocalization in Chemically Doped Conjugated Polymers. *Chem. Mater.* **2021**, *33*, 8489−8500.
49. Arrigoni, A.; Brambilla, L.; Castiglioni, C.; et al. Conducting Electrospun Nanofibres: Monitoring of Iodine Doping of P3HT Through Infrared (IRAV) and Raman (RaAV) Polaron Spectroscopic Features. *Nanomaterials* **2022**, *12*, 4308.
50. Spano, F.C.; Silva, C.H. Aggregate Behavior in Polymeric Semiconductors. *Annu. Rev. Phys. Chem.* **2014**, *65*, 477–500.
51. Hu, K.; Doti, S.; Brambilla, L.; et al. Vibrational Properties of Doped P3HT Chains in Solution: Insight into the Doping Mechanism from Infrared IRAV and Raman RaAV Bands. *Molecules* **2025**, *30*, 1403.
52. Lopez-Navarrete, J.T.; Zerbi, G. Lattice Dynamics and Vibrational Spectra of Polythiophene. I. Oligomers and Polymer. *J. Chem. Phys.* **1991**, *94*, 957–964.
53. Lopez-Navarrete, J.T.; Zerbi, G. Lattice Dynamics and Vibrational Spectra of Polythiophene. II. Effective Coordinate Theory, Doping Induced, and Photoexcited Spectra. *J. Chem. Phys.* **1991**, *94*, 965–970.
54. Baggioli, A.; Meille, S.V.; Raos, G.; et al. Intramolecular CH/π Interactions in Alkylaromatics: Monomer Conformations for Poly(3-alkylthiophene) Atomistic Models. *Int. J. Quantum Chem.* **2013**, *113*, 2154–2162.
55. Su, W.P.; Schrieffer, J.R.; Heeger, A.J. Soliton Excitations in Polyacetylene. *Phys. Rev. B* **1980**, *22*, 2099–2111.
56. Mele, E.J.; Rice, M.J. Vibrational Excitations of Charged Solitons. *Phys. Rev. Lett.* **1980**, *45*, 926–929.
57. Ehrenfreund, E.; Vardeny, Z.; Brafman, O.; et al. Amplitude and Phase Modes in Trans Polyacetylene Resonant Raman Scattering and Induced Infrared Activity. *Phys. Rev. B* **1987**, *36*, 1535–1553.
58. Vardeny, Z.; Ehrenfreund, E.; Brafman, O.; et al. Resonant Raman Scattering from Amplitude Modes in trans-(CH)x and -(CD)x. *Phys. Rev. Lett.* **1983**, *51*, 2326–2329.
59. Painelli, A.; Girlando, A.; Del Freo, L.; et al. Infrared Intensity and Local Vibrations of Charged Solitons. *Phys. Rev. B* **1997**, *56*, 15100–15108.
60. Jacobs, I.E.; Cendra, C.; Harrelson, T.F.; et al. Polymorphism Controls the Degree of Charge Transfer in a Molecularly Doped Semiconducting Polymer. *Mater. Horiz.*, **2018**, *5*, 655–660.
61. Casalegno, M.; Famulari, A.; Meille, S.V. Modeling of Poly(3-hexylthiophene) and Its Oligomer's Structure and Thermal Behavior with Different Force Fields: Insights into the Phase Transitions of Semiconducting Polymers. *Macromolecules* **2022**, *55*, 2398–2412.
62. Vilela Oliveira, D.; Peintinger, M.F.; Laun, J.; et al. BSSE-Correction Scheme for Consistent Gaussian Basis Sets of Double- and Triple-zeta Valence with Polarization Quality for Solid-State Calculations, *J. Comp. Chem.* **2019**, *40*, 2364–2376.
63. Dovesi, R.; Orlando, R.; Erba, A.; et al. CRYSTAL14: A Program for the Ab Initio Investigation of Crystalline Solids. *Int. J. Quantum Chem.* **2014**, *114*, 1287–1317.
64. Dovesi, R.; Erba, A.; Orlando, R.; et al. Quantum-Mechanical Condensed Matter Simulations with CRYSTAL. *Wiley Interdiscip. Rev. Comput. Mol. Sci.* **2018**, *8*, e1360.
65. Dovesi, R.; Erba, A.; Orlando, R.; et al. *CRYSTAL17 User's Manual*; University of Torino: Torino, Italy, 2017.
66. Frisch, M.J.; Trucks, G.W.; Schlegel, H.B.; et al. *Gaussian 09, Revision D.01*; Gaussian Inc.: Wallingford, CT, USA, 2009.
67. Vosko, S.H.; Wilk, L.; Nusair, M. Accurate Spin-Dependent Electron Liquid Correlation Energies for Local Spin Density Calculations: A Critical Analysis. *Can. J. Phys.* **1980**, *58*, 1200–1211.
68. Becke, A.D. Density-Functional Thermochemistry. III. The Role of Exact Exchange, *J. Chem. Phys.* **1993**, *98*, 5648–5652.
69. Lee, C.; Yang, W.; Parr, R.G. Development of the Colle–Salvetti Correlation-Energy Formula into a Functional of the Electron Density, *Phys. Rev. B* **1988**, *37*, 785–789.

70. Gussoni, M.; Castiglioni, C.; Zerbi, G. Vibrational Spectroscopy of Polyconjugated Materials: Polyacetylene and Polyenes. In *Spectroscopy of Advanced Materials*; Clark, R.J.H., Hester, R.E., Eds.; Wiley: New York, NY, USA, 1991; pp. 251–353.
71. Castiglioni, C.; Navarrete, J.T.L.; Zerbi, G.; et al. A Simple Interpretation of the Vibrational Spectra of Undoped, Doped and Photoexcited Polyacetylene: Amplitude Mode Theory in the GF Formalism. *Solid State Commun.* **1988**, *65*, 625–630.
72. Zerbi, G.; Gussoni, M.; Castiglioni, C. Vibrational Spectroscopy of Polyconjugated Aromatic Materials with Electrical Non-Linear Properties. In *Conjugated Polymers*; Brédas, J.L., Silbey, R., Eds.; Springer: Dordrecht, The Netherlands, 1991; pp. 435–507.
73. Castiglioni, C.; Del Zoppo, M.; Zerbi, G. Vibrational Raman Spectroscopy of Polyconjugated Organic Oligomers and Polymers. *J. Raman Spectrosc.* **1993**, *24*, 485–494.
74. Hernandez, V.; Castiglioni, C.; Del Zoppo, M.; et al. Confinement Potential and π-Electron Delocalization in Polyconjugated Organic Materials. *Phys. Rev. B* **1994**, *50*, 9815–9823.
75. Castiglioni, C.; Tommasini, M.; Zerbi, G. Raman Spectroscopy of Polyconjugated Molecules and Materials: Confinement Effect in One and Two Dimensions. *Philos. Trans. R. Soc. A* **2004**, *362*, 2425–2459.
76. Tommasini, M.; Fazzi, D.; Milani, A.; et al. Intramolecular Vibrational Force Fields for Linear Carbon Chains Through an Adaptative Linear Scaling Scheme. *J. Phys. Chem. A*, **2007**, *45*, 11645–11651.